Sedimentology (2007) **54,** 55–70 doi: 10.1111/j.1365-3091.2006.00826.x

Holocene evolution of the Anichab Pan on the south-west coast of Namibia

JOHN S. COMPTON
Department of Geological Sciences, University of Cape Town, Rondebosch 7700, South Africa (E-mail: compton@geology.uct.ac.za)

ABSTRACT

Coastal sediment-filled depressions (pans) are one of the few areas that contain Quaternary records of sea-level and palaeoenvironmental change along the western margin of southern Africa. Anichab is a 128 km^2 salt-encrusted pan on the hyper-arid southern coast of Namibia with an emergent, well-preserved and in-place mid-Holocene mollusc assemblage. The molluscs are typical of subtidal sands on the sheltered side of offshore islands but include several warm-water species no longer found living along this coast. The Holocene evolution of the pan was largely influenced by changes in sea level and supply of sand along the coast. Calibrated radiocarbon ages of mollusc shells indicate a maximum Holocene sea level of *ca* 2 m above mean sea level (msl) from 7·0 to 6·3 ka and a return to near present-day sea level by 5·3 ka. The pan surface is 2 m below msl and has been emergent since 4·9 ka from the build up of sandy beaches and coastal dunes. A thin (1–4 cm) halite crust occurs over much of the pan surface but a layer of halite-cemented sand up to 40 cm thick is restricted to the central pan. Gypsum occurs near the subsurface brine interface and is limited by calcium to the edges of the pan. Nodules of calcite-cemented sand are forming in brackish, relatively high alkalinity subsurface waters in the south-east corner of the pan and nodules of aragonite-cemented sand are forming in brines 1 m below the central pan surface. Although modern dolomite has been reported from coastal lagoons of Brazil and Australia, carbonate cements are a minor feature of Anichab Pan and dolomite was restricted to a single reworked nodule most likely of Late Pleistocene age. Therefore, Anichab Pan does not appear to be a modern analogue to extensive, mixed-water dolomite cements found in Upper Pleistocene sediment-filled depressions on the Namibian shelf.

Keywords Brine, calcite, calibrated radiocarbon ages, coastal pan, dolomite, Holocene, molluscs, sea level.

INTRODUCTION

Coastal pans, lagoons and wetlands (vleis) are some of the few environments where Quaternary deposits are preserved on the semi-arid to hyper-arid south-west coast of Africa. These coastal deposits provide valuable records of Holocene sea level and palaeoenvironments (Miller *et al.*, 1993; Baxter & Meadows, 1999; Compton, 2001, 2006). Sediment-filled shallow depressions (pans) are a common feature of the coast with several dozen pans of variable extent and morphology occurring in South Africa, Namibia and Angola, but few of these pans have been studied. Anichab Pan has many features shared by other coastal pans such as periodic flooding by the sea, wind deflation, groundwater seeps and mobile dune sand. During glacial lowstands the area was subjected to wind erosion to form north–south-oriented bedrock ridges (yardangs) and valleys (yardang troughs). Sea level rose rapidly during the last deglaciation to its maximum position of around +3 m above present-day mean sea level (msl) during the mid-Holocene (Compton, 2001, 2006; Ramsay & Cooper, 2002) and, as a result, emergent mid-Holocene subtidal environments are commonly exposed along the coast.

Coastal lagoons and pans are also often the environments where carbonate cements form including dolomite, a common rock-forming mineral whose modern origins remain poorly understood. The discovery of significant amounts of diagenetic dolomite in offshore sediment-filled basins on the Namibian shelf adjacent to Anichab Pan (Compton *et al.*, 2001) and the report of dolomite forming in modern coastal environments (von der Borch, 1976; Pierre *et al.*, 1984; Vasconcelos & McKenzie, 1997; Wright, 1999) raised the question of whether Anichab Pan is an area of modern dolomite formation. In this paper the Holocene evolution of Anichab Pan is investigated based on the composition of cored sediment and the radiocarbon ages of mollusc shells. In addition, the geochemistry of subsurface pan waters and cements is used to evaluate to what extent Anichab Pan may provide a modern analogue to the origin of older diagenetic carbonates in offshore shelf deposits.

GEOLOGICAL SETTING

Anichab Pan is located on the south-west coast of Namibia, 60 km north of the coastal town of Lüderitz (Fig. 1). The pan surface, at around 2 m below msl, occupies an area of *ca* 128 km^2. The eastern margin of the pan is covered by 20–60 m high mobile dunes of the Namib Sand Sea. Precambrian gneissic outcrops (Kröner & Jackson, 1974) rise to elevations of 45 m along the western margin of the pan. The resistant Precambrian rocky outcrops define a north–south trending yardang peninsula with Hottentots Bay to the north and a large coastal embayment to the south as far as Lüderitz. The diamondiferous beach

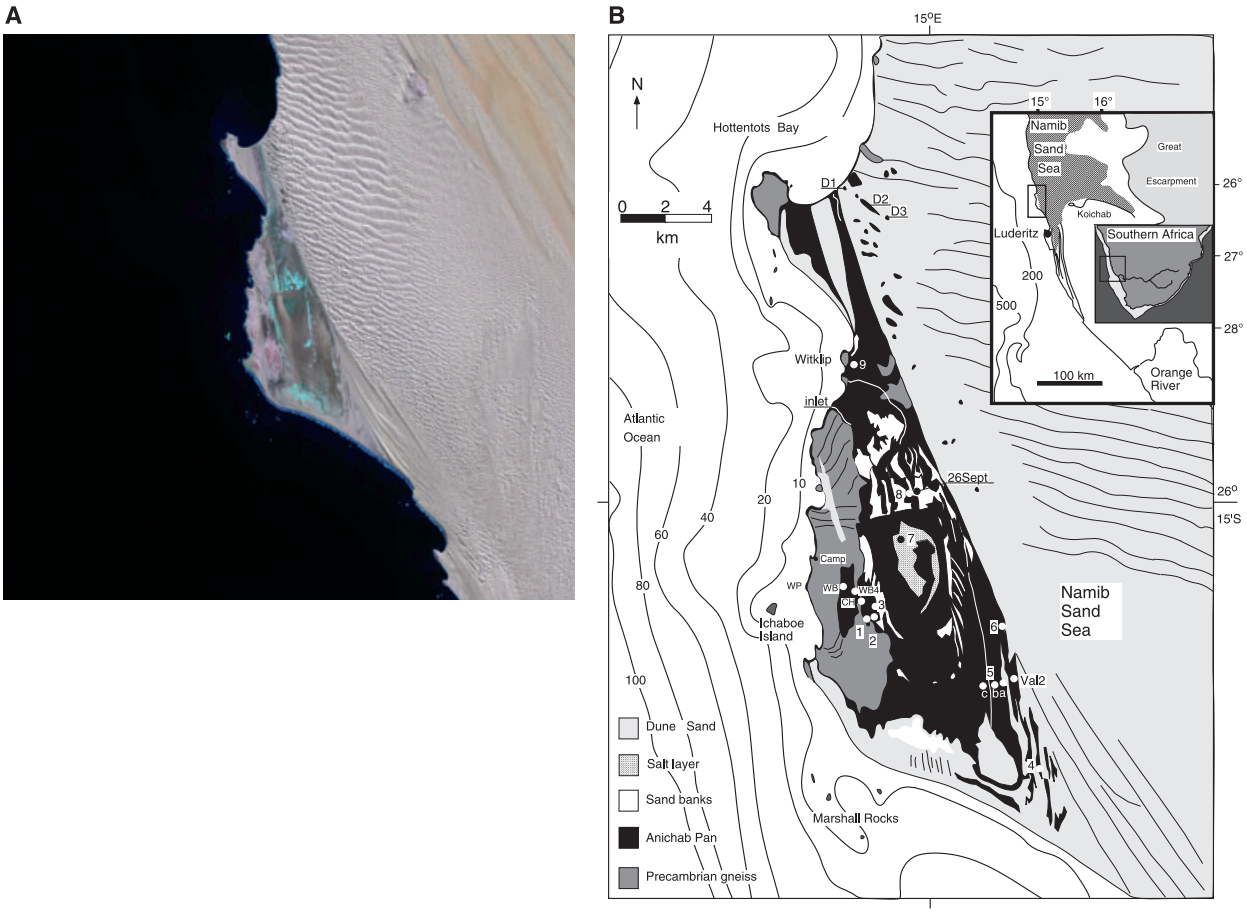

Fig. 1. (A) Landsat 7 Enhanced Thematic Mapper image at 30 m resolution from the Global Land Cover Facility (University of Maryland) showing features of the Anichab Pan area. Image taken in July 1999 with bands 7, 4 and 2 displayed in red, green and blue. Blue colours reflect shell-covered sandbank areas. (B) Map of the study area showing the regional context of southern Africa and the Orange River, the Namib Sand Sea and the town of Lüderitz. The main map shows Anichab Pan in black with the Namib Sand Sea to the east and the Precambrian basement rock ridge to the west. Sample sites are indicated by numbers and letters. Land features based on 1:80 000 aerial photography (1998) from the Namibian Survey Office, Windhoek and bathymetry from Rogers (1977).

gravels surrounding Anichab Pan are situated in the highly restricted Sperrgebiet area of southern Namibia and as a consequence little is known of the geology of the pan area (Kaiser, 1926; Kröner & Jackson, 1974). Annual temperatures range from 5 to 30 °C and rainfall ranges from 5 to 10 mm with significant additional precipitation as coastal fog. There are no rivers draining into the pan and no tidal inlets connecting it to the sea. Strong, southerly winds blow during the summer months to form partially vegetated coastal dunes and some mobile dune cordons extend north towards Hottentots Bay. Vegetation is sparse and restricted to rocky outcrops, coastal dunes and dune troughs located in the south eastern area of the pan. Most of the pan has a dark brown, 1–4 cm thick irregular salt-encrusted surface with moist sand immediately below and water-saturated sand 10–40 cm below the surface. Polygonal desiccation cracks are common and an up to 40 cm thick salt crust is present in the central pan. Vegetation on the pan surface is limited to filamentous algal mats. Rising 1–2 m above the flat pan surface are sandbanks, many of which are covered by mollusc shells (Fig. 1).

METHODS

Sediment and subsurface water samples were collected in the Anichab Pan area at the end of September 2001 (Fig. 1B). Although the pan floods on occasion after rainfall or periods of high seas, there was no standing water in the pan at the time of sampling. Sediment was recovered in aluminium vibracores with a maximum recovery of 4·5 m below the pan surface. Vibracores were split and described within 48 h of recovery.

Subsurface water samples were collected at the top of the water table from pits dug below the pan surface. Water sample numbers (Table 1) correspond to the coring site adjacent to where they were collected. Subsurface pan waters were filtered through a 0·45 μm cellulose acetate membrane filter and titrated within 24 h of recovery. Water densities were determined by weighing 10 ml (glass pipette) of sample at 20 °C. Ion chromatography (IC) was used to determine major ion concentrations, except Ca, which was measured using atomic absorption spectrometry. Sr concentration and isotope composition were determined by inductively coupled plasma mass spectrometry. The degree of uncertainty is reflected in the duplicate analyses of several samples and of a seawater sample collected at Wreck Point (Table 1). The uncertainty of the analyses is large because of the up to 10 000 time dilutions that were required for analysis of the brine samples. The Cl values of the Wreck Point seawater sample are too high and suggest that the negative imbalance of the water samples results from uncertainty in the IC Cl measurements rather than the presence of an unmeasured cation.

Table 1. Major ion chemistry of subsurface waters of Anichab Pan (mmol kg^{-1}).

Sample	g cm^{-3}	pH	Na	Ca	Mg	K	Sr	Cl	SO_4	Alk	Mg/Ca	%Charge	*I*
1	1·21	6·60	3642	13	583	96	0·16	4950	154	nm	46	−3·2	5·8
2	1·20	nm	3293	12	566	92	0·17	4829	161	nm	46	−6·3	5·6
3	1·19	nm	2938	14	481	109	0·14	4344	154	2·8	33	−7·1	5·0
4	1·00	7·55	57	5	6	1	0·04	73	2	4·6	1	−2·1	0·1
5a	1·07	7·26	1344	23	261	23	0·37	1972	49	2·2	11	−3·4	2·3
5a(D)		nm	1372	nm	172	25	0·25	1911	53	2·2	nm	nm	nm
5c	1·21	6·19	2956	105	923	49	1·21	5143	80	0·4	9	−2·3	6·3
6	1·04	7·50	690	17	91	12	0·14	975	14	2·1	5	−4·5	1·1
7	1·20	6·70	3663	3	329	60	0·23	4915	109	nm	124	−7·8	5·2
8	1·20	6·89	3703	20	409	70	0·22	4905	119	1·6	20	−5·3	5·4
9	1·21	6·96	3363	11	508	84	0·14	4728	187	2·5	48	−6·5	5·5
9(D)		nm	3503	nm	567	86	0·14	4831	190	2·5	nm	nm	nm
WB	1·13	6·87	1900	39	482	91	0·21	3048	85	nm	12	−2·9	3·7
D1	1·03	8·00	569	13	72	12	0·11	698	36	1·2	6	−1·4	0·9
D2	1·04	7·54	631	17	58	14	0·14	823	41	1·9	3	−6·5	1·0
D3	1·05	7·46	905	16	110	22	0·11	1114	44	1·7	7	−1·0	1·4
WP	1·02	8·13	445	10	48	10	0·14	571	32	nm	5	−5·2	0·7
WP(D)			464	nm	55	10	0·08	585	31	nm	nm	nm	nm

D = duplicate analysis (mean value plotted on figures); nm = not measured; WP = Wreck Point seawater sample. Water sample numbers correspond to core site numbers.
% charge = (difference in cation and anion charges/total charge) × 100; I = ionic strength = $0{\cdot}5\Sigma_i c_i Z_i^2$.

The mineralogy of the sediment and cemented nodules was determined using a Philips X-ray diffractometer at the University of Cape Town (UCT). Grain size was determined using sieves and by settling column on the sand-size fraction. Cemented sediment samples were examined using the scanning electron microscope (SEM) facility at UCT. Stable isotopes were measured at UCT using a Finnigan MAT 252 mass spectrometer after off-line reaction in 100% phosphoric acid at 25 °C. Isotope data were normalized to Peedee Formation belemnite (PDB) using an internal standard calibrated against NBS-19 with reproducibility better than 0·1‰ for $\delta^{13}C$ and 0·2‰ for $\delta^{18}O$.

Conventional radiocarbon ages were determined on bulk shell samples by the Quaternary Dating Laboratory in Pretoria. Radiocarbon age can differ significantly from calendar age because of variations in the ^{14}C production in the atmosphere (Hughen *et al.*, 2004). In addition, radiocarbon ages of marine shell samples must be corrected for the age of the ocean carbon reservoir, especially in areas of upwelling (Stuiver & Braziunas, 1993). Calibrated ages along with their 2σ range were obtained using the WC93 program (Talma & Vogel, 1993) which assumes a constant mean reservoir age of 550 years for upwelled south-east Atlantic coastal waters and applies the marine data set of Stuiver & Braziunas (1993). Paired charcoal and shell radiocarbon dates from coastal archaeological sites indicate a reservoir age of around 550 years (Tonner, 2003), but variation in the reservoir age is likely in response to changes in upwelling intensity and other factors, and would increase the uncertainty of the reported calibrated ages. Shell samples were first screened for any indication of recrystallization or alteration based on texture (etched or pitted surfaces), mineralogy (aragonite versus calcite; encrusted gypsum) and stable isotopes (low carbon and oxygen isotope values). Only samples that showed no signs of alteration were submitted for radiocarbon analysis.

RESULTS

Stratigraphy and facies

A series of vibracores were recovered from the pan that range in length from 0·5 to 4·5 m (Figs 2–4). The sediment throughout the study area is dominated by quartzose sand that contains between 0·5 and 10 wt% quartzose mud. Sand grains vary in size from fine to very coarse. Fine to medium grains are angular to subrounded whereas coarse to very coarse grains are subrounded to rounded. Feldspar makes up between 10% and 15% and carbonate shell fragments generally <2% of the sand grains. The gravel fraction includes mollusc shells and shell fragments, as well as nodules of carbonate-cemented sand and gypsum crystals in some cores. Many of the molluscs occur on the pan surface as whole, articulated shells in life position partially exhumed by wind deflation of the loose sand surrounding them. Mollusc shells are generally far less abundant in the subsurface sediments where they commonly occur as fragmented debris. The extent of alteration of surface and subsurface shells is variable and includes pitted and etched surfaces, orange staining by iron oxides and cementation by gypsum.

Western pan area

Within the Precambrian basement rock on the western margin of the pan is a sediment-filled embayment (Fig. 1B). On the western margin of this embayment (Site WB), the sediment in a 70 cm deep pit dug to the water table consists of medium to coarse orange/brown sand with scattered shell. The shell content increases upcore into a 20 cm thick sandy shelly gravel that contains abundant and mostly articulated bivalves (*Dosinia lupinus* and *Solen capensis*) partially cemented by gypsum and halite. On the eastern side of the embayment (Site WB4) the water table was 40 cm below the pan surface, and the dark brown medium to coarse quartzose sand lacked shell except where it bordered Precambrian bedrock. The articulated clam *Gastrana matadoa* occurs nestled among the *in situ* large barnacle *Austromegabalanus cylindricus* 1·5 m above the pan surface at Site WB4 (Fig. 2). The exposed tidal channel cut into Precambrian bedrock connecting the embayment to the main pan (Site CH) is floored by a shell hash made up of a mixture of reworked barnacle fragments and the oyster *Ostreola stentina* as well as echinoderm plates and spines, foraminifera, ostracods and worm tubes (Table 2). This oyster–barnacle hash extends from the channel out onto the pan and was recovered in Core 1 at 1·3 m and at the base of Core 2 associated with green muddy sand (Fig. 2). A specimen of an intact displaced oyster shell collected 20 cm below the channel surface has a calibrated radiocarbon age of 7·0 ka and *in situ* barnacles from Site WB4 have a calibrated age of 6·6 ka (Table 3).

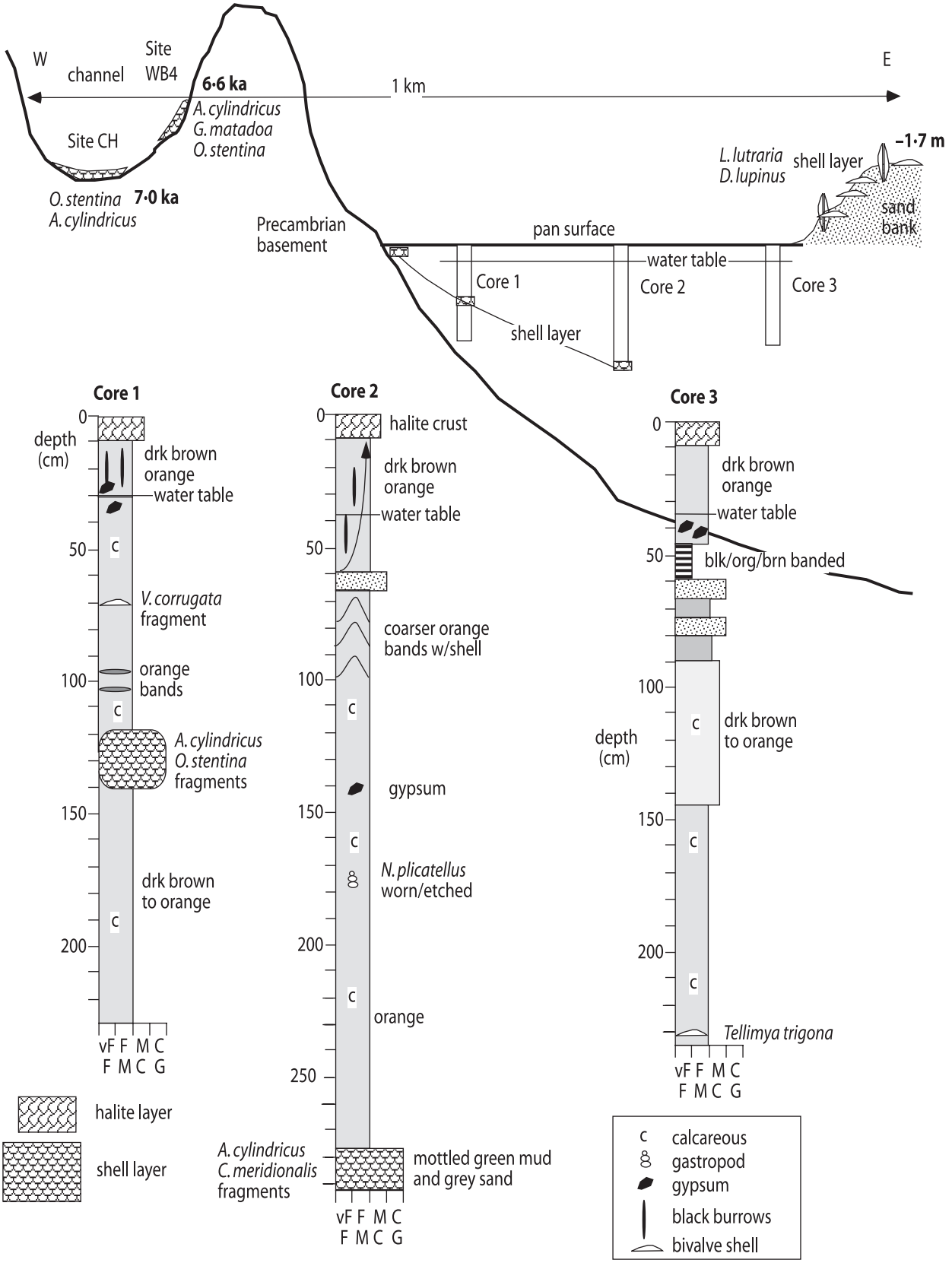

Fig. 2. Stratigraphy of cores 1, 2 and 3 placed within a schematic cross-section of the western embayment channel and pan. The predominant grain size of the cored sediment is indicated (legend on Fig. 3).

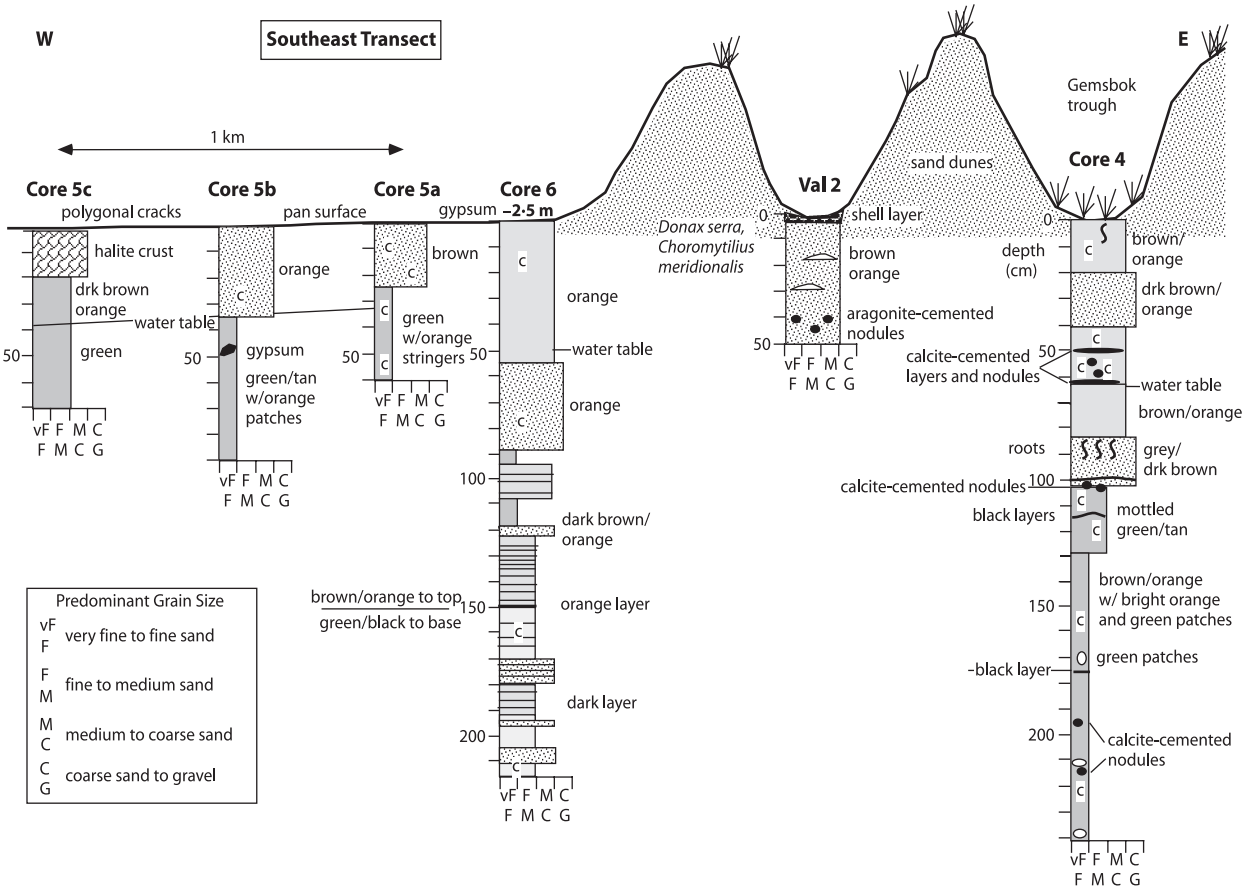

Fig. 3. Stratigraphy of cores 4, 5 and 6 placed within a schematic cross-section of the south-eastern area of the pan. Core 4 and Val2 pit occur in the troughs of mobile dunes. Cores 5 and 6 are from the pan surface. The predominant grain size of the cored sediment is indicated.

Cores 1, 2 and 3 consist of fine to medium brown to orange slightly calcareous quartzose sand. Medium to coarse sand layers occur at 0·5–1 m in cores 2 and 3 (Fig. 2). Tabular gypsum crystals containing abundant quartz grains occur at the water table located 35 cm below the pan surface. Adjacent to cores 1, 2 and 3 are sandbanks rising 2 m above the pan surface. These sandbanks consist of brown and orange, fine to medium sand capped by a 20–30 cm thick sandy shelly gravel containing 80% *Dosinia lupinus* and 20% *Lutraria lutraria* shells of which approximately half are articulated.

South-eastern area of the pan

The south-east corner of the pan has a brackish water seep (sample 4; Table 1). No standing water was observed, but moist soils with abundant reed-like vegetation occur in the dune troughs where four gemsbok antelope were observed feeding and digging into the sand to access subsurface water. Core 4, taken in a dune trough, recovered 2·4 m of orange to dark brown quartzose sand (Fig. 3). The sand in Core 4 grades upward from a very fine sand with green patches and dark organic-rich layers at the base into a fine green and tan mottled sand overlain by medium to very coarse orange/brown sand. Nodules of calcite-cemented sand were recovered at 2·1, 1·9 and 1·1 m, and an irregular shaped 2–3 cm thick bed of calcite-cemented sand from 0·5 to 0·6 m core depth. The bed of calcite-cemented sand contains root casts and the base of the bed coincides with the water table at 0·6 m.

North of Core 4, shell-rich areas were found on the surface of the dune troughs in the vicinity of Site Val2 (Fig. 1B). A dry pit was dug at Site Val2 where nodules of aragonite-cemented sand were recovered at 40–50 cm and shelly sand from 20 to 30 cm below the surface. The shell on the surface and subsurface consists of transported white clams (*Donax serra*) and black mussel fragments (*Choromytilus meridionalis*) similar to shells found on the modern south-facing beach of the

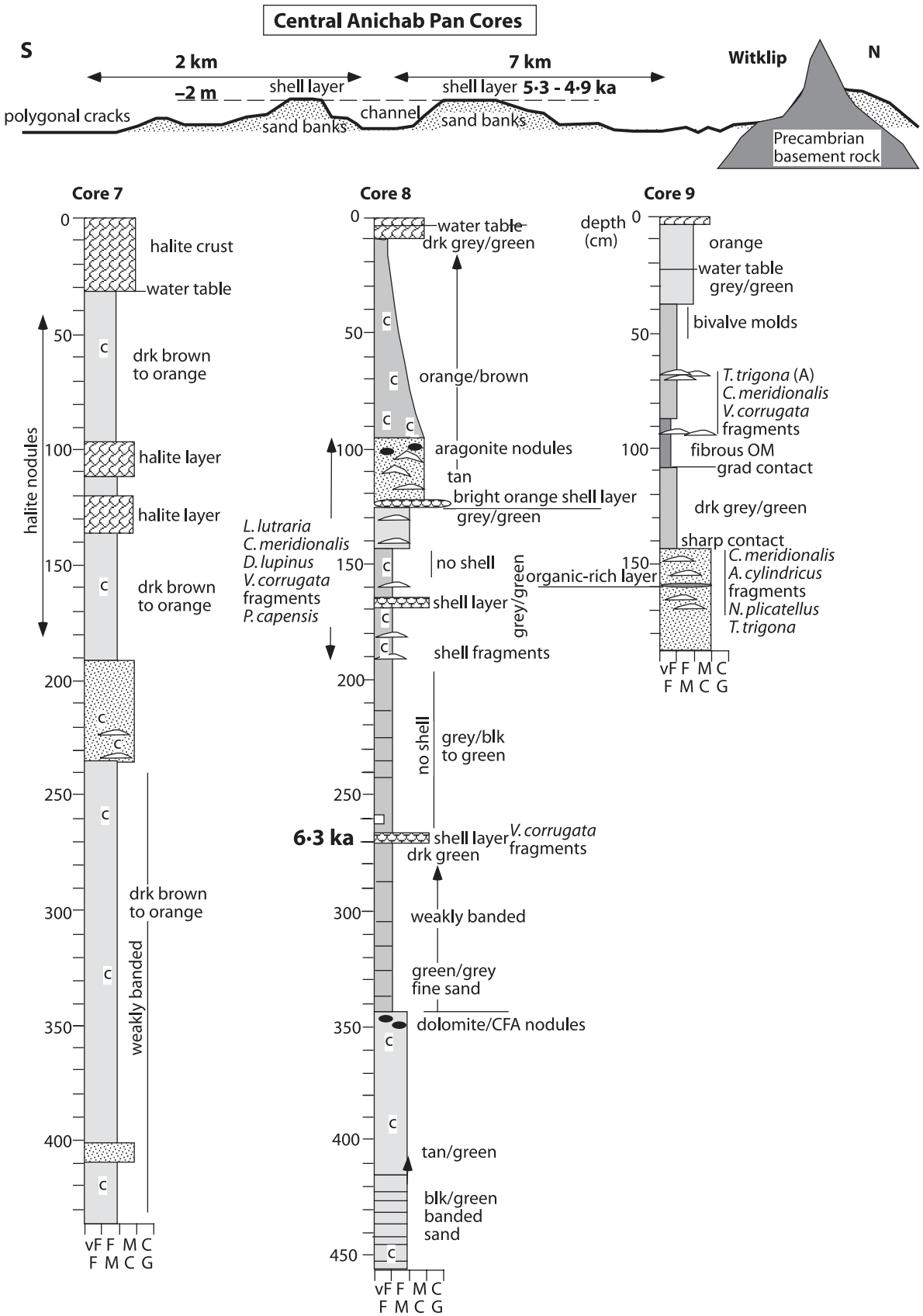

Fig. 4. Stratigraphy of cores 7, 8 and 9 placed within a schematic cross-section of the central pan area. The predominant grain size of the cored sediment is indicated (legend on Fig. 3).

Table 2. Mollusc and foraminifera assemblages on the surface of Anichab Pan.

Sample site	Fossil assemblage
Salt crust (Cores 1, 2, 3, 7, 8, 9)	Halite layer, polygonal cracks; no fossils (bivalve moulds at 40–50 cm in Core 9)
Gypsum crust (100 m west of Core 6)	*Fasciolaria lugubris lugubris* (P), *Crepidula porcellana* (P), *Protomella capensis* (C), *Solen capensis* (P),*Gastrana matadoa* (P), *Dendrofissurella scutellum* (P)
Sandbanks	
Adjacent to Core 3	*Dosinia lupinus* (A), *Lutraria lutraria* (A), *Venerupis corrugata* (P), *Bullia laevissima* (P)
Adjacent to Core 8: 26Sept	*Lutraria lutraria* (A), *Venerupis corrugata* (adult and juvenile) (A), *Choromytilus meridionalis* (fragments) (C), *Carditella laticosta* (P), *Dosinia lupinus* (P), *Tellimya trigona* (C), *Nassarius plicatellus* (A), *Crepidula porcellana* (A), *Protomella capensis* (A), *Prunum capensis* (P), *Elphidium* cf. *advenum*, ostracods (marine), echinoid plates/spines
Western embayment	
Western margin (site WB)	*Dosinia lupinus* (A), *Solen capensis* (C)
Eastern margin (1·5 m above pan surface)	*Austromegabalanus cylindricus* (A), *Gastrana matadoa* (articulated) (A), *Ostreola stentina* (P), *Dendrofissurella scutellum* (P), *Quinqueloculina* cf. *seminulum*, *Ammonia* cf. *japonica, Elphidium* cf. *advenum*, ostracods (marine), echinoid plates/spines, calcareous worm tubes
Channel (site CH)	*Ostreola stentina* (A), *Austromegabalanus cylindricus* (A) *Miliolinella subrotunda, Quinqueloculina* cf. *seminulum*, *Ammonia* cf. *japonica*, *Elphidium* cf. *advenum*, ostracods (marine), echinoid plates/spines, calcareous worm tubes
Protected rocky shores (western margin of pan)	*Austromegabalanus cylindricus* (A), *Argobuccinum pustulosum proditor (C)*, *Burnupena* sp. (C), *Nassarius plicatellus* (P), *Prunum capensis* (P), *Gastrana matadoa* (P)
Dune troughs (D1, 2, 3)	*Lutraria lutraria* (fragments) (C), *Choromytilus meridionalis* (fragments) (C), *Helicon dunkeri* (P), *Argobuccinum pustulosum proditor* (P), *Nucella dubia* (P), *Burnupena* sp. (P)
Dune trough (Val2)	*Donax serra* (A), *Choromytilus meridionalis* (fragments) (C)

A = abundant, C = common, P = present. Identification of molluscs from Branch & Branch (1981), Kilburn & Rippey (1982) and Branch *et al.* (1994).

Table 3. Radiocarbon analyses of shell material from Anichab Pan.

Sample	Material	Analytical No. Pta-	$\delta^{13}C$ ‰ PDB	Conventional ^{14}C age	Calibrated ^{14}C age (2σ range)
VAL2	*Donax serra* (T)	8629	0·2	990 ± 50	471 (386–524)
26SEPT	*Lutraria lutraria* (I)	8633	1·3	5180 ± 70	5336 (5245–5552)
26SEPT	*Lutraria lutraria* (I)	9184	1·1	5060 ± 70	5252 (4996–5409)
26SEPT	*Gastrana matadoa* (I)	9180	1·4	4840 ± 50	4867 (4813–5022)
CH	*Ostreola stentina* (T)	8635	0·4	6640 + 70	6961 (6797–7143)
WB4	*A. cylindricus* (I)	9182	1·1	6310 + 50	6604 (6461–6707)
Core 8 (2·7 m)	*V. corrugata* (T)	GrA-25207	−1·8	5985 + 40	6254 (6174–6307)

Ages are in years Before Present (yr BP). (T) = transported shell; (I) = in place shell. Calibrated ages are from Talma & Vogel (1993) and Stuiver & Braziunas (1993).

pan. A transported *D. serra* shell from 30 cm below the surface at Site Val2 has a calibrated radiocarbon age of 0·5 ka (Table 3).

West of Site Val2, three pits were dug below the pan surface at sites 5a, b and c (Fig. 1B). The water table occurs at 32 cm below the surface at Site 5a in basal calcareous green fine sand that is in sharp contact with overlying calcareous orange/brown medium sand (Fig. 3). Site 5b is *ca* 200 m west of Site 5a and consists of basal very fine green and tan mottled sand capped by coarse orange sand. The top medium to coarse sand is slightly calcareous and gypsum crystals were recovered at 45 cm sediment depth. Site 5c is *ca* 500 m west of Site 5b and has polygonal desiccation cracks on the surface. Site 5c consists of a green fine to medium basal sand in gradational contact with fine orange sand and is capped by a

20 cm thick halite layer (Fig. 3). The water table occurs at 38 cm below the surface at Site 5c. The sediment at Site 5c is non-calcareous and non-gypsiferous. Core 6 was taken *ca* 3 km north of Site 5a on the eastern edge of the pan where it borders the Namib Sand Sea (Fig. 1B). The base of Core 6 consists of fine to medium and medium to coarse slightly calcareous green black sands. An orange sand layer at 1·5 m marks the abrupt transition to the overlying dark brown and orange very fine to fine and medium to very coarse sands (Fig. 3). The sand is banded throughout much of the lower half of Core 6. No gypsum or shell was recovered in Core 6, but 100 m west is a 10 cm thick gypsum layer on the pan surface with a scattered, diverse mollusc assemblage (Table 2).

Central pan area

Three cores were recovered from the central Anichab Pan (Figs 1 and 4). Core 7 is from a large central depression covered by a 30–40 cm thick halite crust. Sediment in Core 7 consists of a fine to coarse dark orange to brown slightly calcareous sand. The lower sands are weakly banded and shell was only recovered in a medium to coarse sand at 2·2–2·3 m. Nodules and layers of halite-cemented sand occur 1·8 m below the surface. No gypsum was detected in Core 7. Core 8 occurs *ca* 2 km north of Core 7 in a channel bordered by 1–2 m high sandbanks. The base of Core 8 consists of slightly calcareous fine to medium sand that grades from black and green banded sand into a homogeneous tan-green sand that is capped by dolomite and carbonate fluorapatite (CFA) cemented, diatomaceous laminated nodules at 3·45 m (Fig. 4). The overlying faintly banded green-grey fine sand becomes increasingly dark green upcore and is capped by a shell layer of *Venerupis corrugata* fragments with a calibrated radiocarbon age of 6·3 ka. The shell layer is overlain by weakly banded, grey black to green fine sands. Shell fragments (predominantly *L. lutraria*) occur above 1·9 m. The fine sand grades into grey-green medium sand up to a bright orange shell hash layer at 1·25 m. The orange shell hash layer is overlain by a tan medium to coarse shelly sand that contains nodules of aragonite-cemented sand near the top. Calcareous orange-brown medium sand fines upcore into a fine dark grey-green sand that is capped by a 10 cm thick halite crust.

The adjacent sandbanks have a concentrated shell layer extending to 20 cm subsurface with a diverse mollusc assemblage that includes abundant *L. lutraria*, *V. corrugata*, *N. plicatellus*, *C. porcellana* and *P. capensis* (Table 2). Some shell surfaces are pitted, sand blasted or stained by iron oxides. The calibrated radiocarbon ages of unaltered, in place and articulated *L. lutraria* and *G. matadoa* from the sandbank surface immediately to the east of Core 8 (Site 26SEPT) range from 4·9 to 5·3 ka (Table 3). Core 9 was recovered 7 km north of Core 8 from a low lying area just east of the Witklip Precambrian outcrop (Fig. 1B). The basal medium to coarse sand contains molluscs and a 1-cm-thick organic-rich layer in sharp contact with the overlying fine sand which grades upcore into a very fine organic-rich sand (Fig. 4). Mollusc shells found between 95 and 70 cm depth are dominated by the white bivalve *Tellimya trigona* and fragments of *V. corrugata*. The fine sand grades upcore into a fine and then medium sand with bivalve moulds at depths of 40–50 cm. The dark grey-green sediment changes to orange across the water table at depths of 22 cm. At the northern end of the pan adjacent to Hottentots Bay three pits were dug to sample the water table 70 cm below the surface of several dune troughs. The dune troughs are surrounded by 60–80 m high mobile dunes and are floored by moist dark orange-brown medium sands. Mollusc shells were present in places on the dune trough surfaces (Table 2).

Chemistry of subsurface pan waters

The majority of subsurface pan waters are brines with an ionic strength (I) that ranges from 2·3 to 6·3 (Table 1). Saline ($I = 0{\cdot}88$–$1{\cdot}36$) subsurface waters occur along the eastern edge of the pan and brackish ($I = 0{\cdot}09$) water occurs in the south-eastern corner at Site 4 (Fig. 1B). The pH of brine waters ranges from 6·2 to 7·3, while the pH of brackish-saline waters ranges from 7·5 to 8·0 (Fig. 5). The dominant ions are Na, Cl, Mg and SO_4. The concentration of the major ions are plotted against Cl, which behaves conservatively up to halite precipitation (Fig. 5). The Na:Cl molar ratio of brackish to saline waters is similar to that of seawater (0·86), but brine waters and one saline sample from Site 6 have Na:Cl molar ratios less than seawater (0·56–0·75). Sites with Na:Cl ratios less than seawater have a 4–35 cm thick halite crust or are adjacent to such sites (sites 6, 5a and WB) and reflect the 1:1 ratio of removed Na and Cl by precipitation of halite.

Sulphate concentrations are generally depleted with respect to seawater with the exception of saline water at sites D1–D2 which has concentrations similar to seawater (Fig. 5). Potassium is

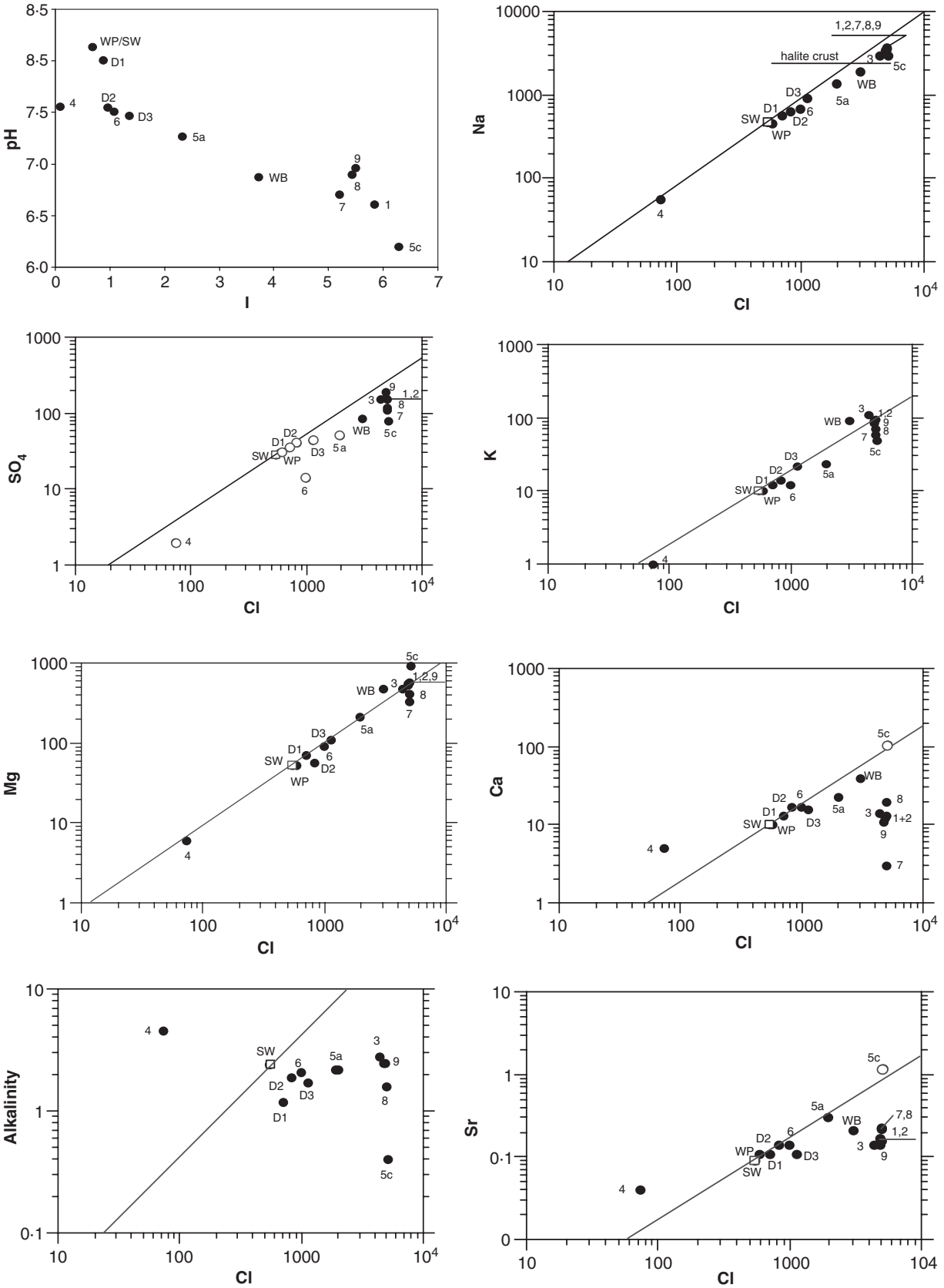

Fig. 5. Subsurface pan water pH plotted against ionic strength (*I*) and major ion concentrations plotted against chloride ion concentrations (mmol kg^{-1}). Filled circles in sulphate ion plot are brine samples (I > 3).

Table 4. Isotope composition of carbonate from Anichab Pan.

Sample	Material	$\delta^{13}C$ ‰ PDB	$\delta^{18}O$ ‰ PDB	$^{87}Sr/^{86}Sr$
26SEPT	*Lutraria lutraria*	0·92	1·76	0·709 ± 0·001
CH	*Ostreola stentina*	0·71	0·88	0·709 ± 0·001
Core 4 (0·6 m)	Calcite cement	−2·28	−1·35	0·710 ± 0·001
Core 4 (1 m)	Calcite cement	−6·96	0·87	0·711 ± 0·002
Core 4 (0·7 m)	Subsurface water			0·710 ± 0·001
Core 8 (1 m)	Aragonite cement			0·716 ± 0·002
Core 8 (3·5 m)	Dolomite cement			0·714 ± 0·001

depleted relative to seawater in brackish and saline pan waters, but similar to seawater for the three dune valley samples (D1–D3). K:Cl molar ratios are highly variable for brine waters, with less-than-seawater ratios to the east and greater-than-seawater ratios to the west at sites adjacent to Precambrian gneiss outcrops. Magnesium concentrations generally fall on the seawater line except for brine samples which have both depleted and enriched ratios relative to seawater. Mg/Ca ratios range from 1 to 124. The Ca:Cl ratio is highest in the brackish water, similar to seawater in saline waters and significantly depleted relative to seawater in brine waters (Fig. 5). Alkalinity is greater-than-seawater in the brackish water sample and generally depleted in saline and brine waters with the lowest alkalinity in brine water from carbonate-free sediment at Site 5c. Sr follows Ca and $^{87}Sr/^{86}Sr$ ratios of pan water from Site 4 and carbonate cements of cores 4 and 8 are similar to or higher than seawater (Table 4).

DISCUSSION

Holocene evolution of Anichab Pan

An emergent coast combined with an arid climate has resulted in an unusually well-preserved mollusc assemblage at Anichab Pan with many of the mollusc shells in life position, exposed by wind deflation as articulated shells on the surface of the pan. The Holocene evolution of palaeoenvironments and sea-level fluctuations as recorded at Anichab Pan is inferred from radiocarbon dating of both in place and locally transported mollusc shells and from the sedimentology of the recovered cores.

The difference in elevation between the time the subtidal (<2 m water depth) oysters and intertidal (±1 m water depth) barnacles were living and their present-day elevation at the embayment sites CH and WB4 indicates that sea level was *ca* 0·5–2 m above present-day msl from 7·0 to 6·6 ka (Fig. 2). The oyster *O. stentina*, which currently lives in warm coastal waters of Angola, the salinity tolerant clams *G. matadoa* and *S. capensis*, which are currently restricted to warmer waters of the south coast of South Africa, (Kilburn & Rippey, 1982; Branch *et al.*, 1994), and the dominant microfossil *Quinqueloculina* cf. *seminulum* indicate that the western embayment had warm, perhaps hypersaline waters. The salinity tolerant clams *G. matadoa* and *S. capensis* (but no oysters) are also found in protected lagoonal waters of Bogenfels Pan located 140 km to the south of Anichab Pan associated with the mid-Holocene highstand (Compton, 2006).

The marine transgression during final deglaciation flooded protected, hard-substrate coastal embayments and provided pockets along the west coast of southern Africa where oysters thrived briefly during the mid Holocene (7·0–6·6 ka). For example, the oyster *Ostrea atherstonei* was recovered in abundance along with *S. capensis* (but not *G. matadoa*) from palaeochannels of the Langebaan Lagoon 840 km south of Anichab Pan. A calibrated radiocarbon age of 6·8 ka of the oyster bed indicates an up to +3 m mid-Holocene highstand at Langebaan Lagoon (Compton, 2001). In addition to protected, rocky substrates, these oyster-rich deposits may reflect increased incursion of warm Agulhas Current water north into Langebaan Lagoon and warm Angola Current water as far south as the Anichab area along the Namibian coast during the mid-Holocene Climatic Optimum.

During maximum flooding of up to +3 m above present-day msl in the mid Holocene, the Precambrian outcrops formed an island and the shelly sandbanks now exposed on the pan surface were submerged and protected by a subtidal seaway with a coastline to the east now buried beneath the Namib Sand Sea (Fig. 1). The sandy subtidal palaeoenvironments of the seaway supported a diverse mollusc assemblage (Table 2)

largely similar to that observed today in the sheltered sandbanks of Possession Island 40 km south of Lüderitz offshore from Elizabeth Bay and Robben Island 10 km offshore from Cape Town. The sandbank environments of these islands leeward of the predominant south–south-west swell are dominated by the large, immobile white clam *L. lutraria* and the clam *V. corrugata* as well as the gastropods *N. plicatellus* and *P. capensis*, which burrow in clean sand (Branch *et al.*, 1994). The black mussel *C. meridionalis* only occurs as fragments and this suggests that it was transported into Anichab Pan from adjacent high-energy, intertidal rocky coastlines.

Subtidal molluscs inhabited the sandbanks of the pan from at least 6·3 ka as indicated by the radiocarbon age of locally transported *V. corrugata* shells recovered at 2·7 m depth in Core 8 (Fig. 4). The age of the youngest in place mollusc assemblage on the exposed sandbank surfaces indicates that a coastal seaway only existed to 4·9 ka based on the calibrated age of an articulated, in place *G. matadoa* shell from site 26SEPT (Table 3). The older shells from the more elevated western embayment and the up to 2 m below msl elevation of the sandbank surfaces suggest that sea level fell to within ±1 m of present-day msl during the final occupation of the coastal seaway from 5·3 to 4·9 ka.

Since 4·9 ka the pan does not appear to have been reoccupied by the sea despite its present-day 2 m below msl elevation. In addition, wind deflation of the sandbank surfaces since exposure at 4·9 ka may have contributed to the lowering of their present-day elevation, although the amount of deflation appears limited by the armouring effect of the shells. In combination with the marine regression between *ca* 6·5 and 5·5 ka documented for this coast (Compton, 2001, 2006), the emergence of the pan surface after 4·9 ka may have resulted from the build up of sandy beaches and coastal dunes. Sandy beaches and dunes currently have crest elevations of between 2 and 6 m above msl at the southern and northern inlets of the pan and these prevent the pan from being flooded by the sea today. The pan is only partially flooded by episodic high seas at an inlet south of Witklip and the beach at Hottentots Bay (Fig. 1B) or after heavy rainfall.

The mollusc assemblage recovered from Core 8 is similar to that of the younger, adjacent sandbanks (Table 2). In Core 8, however, the shells are largely present as fragments and most likely were derived by reworking of shell off the shallow sandbanks to deeper channels. Shell concentration drops off rapidly with depth on the sandbanks and the concentrated shell layer on the surface armours the underlying sand from further wind deflation. The similar composition and uniform and well sorted grain size of sand from the sandbanks suggest that they were originally sand dunes reshaped by subtidal submergence during the mid-Holocene highstand. Much of the pan surface adjacent to the sandbanks has not been deflated but filled in with sand since emergence as indicated by the up to 2·5 m of sand cover over the mid-Holocene shell layers in cores 1, 2 and 8 (Figs 2 and 4). This additional sand accumulation may have occurred when the pan was partially flooded because most sand blown off the southern beach bypasses the salt encrusted surfaces of the pan as well as the shell-armoured sandbanks.

In summary, similar to the Holocene sea-level record of other areas of the west coast of southern Africa (Miller *et al.*, 1993; Compton, 2001, 2006), the Anichab Pan area was initially flooded by the sea-level rise at the end of deglaciation (8–7 ka). Maximum sea level was reached around 7 to 6·6 ka at *ca* 3 m above present-day msl with warm water protected embayments and clean subtidal seaway sand environments formed from modification of flooded aeolian dunes leeward of the Precambrian bedrock island. Sea level then dropped to near its present-day position by 5·3 to 4·9 ka in response to margin uplift predicted by glacio-hydro-isostatic models (Clark & Lingle, 1979; Fleming *et al.*, 1998). The build up of beach and dune sand deposits at the southern and northern ends of the pan as well as the migration of the Namib Sand Sea dunes from the south and east during the marine regression resulted in the subtidal pan surface being emergent since *ca* 4·9 ka.

Cementation of pan sediments

Nodules of carbonate-cemented sand occur mostly along the south-east edge of the pan (sites 4 and Val2; Fig. 3), and at Site 4 are associated with brackish subsurface waters relatively high in Ca and alkalinity (Fig. 5). The low carbon isotope values (Table 4) and the presence of root casts in carbonate nodules from Core 4 suggest that calcite precipitation was promoted by degradation of soil organic matter (Ehleringer, 1989). The only other cored site found to contain nodules of carbonate-cemented sand was in shell-rich sand 1 m below the central pan surface at Site 8 (Fig. 4). Therefore, carbonate precipitation in the pan appears to be limited by the low alkalinity of subsurface brine

waters and the generally low organic matter content of recovered pan sediments.

Gypsum is far more abundant than carbonate cement and is focussed near the water table on the edges of the pan. Gypsum precipitation is limited by the availability of calcium in subsurface waters (Fig. 5), but significant calcium can be derived from carbonate shells, as evidenced by gypsum bivalve moulds and gypsum encrusting and replacing mollusc shells. Halite-cemented sands generally increase in thickness towards the centre of the pan (up to 40 cm thick at the surface of Core 7; Fig. 4) where they generally lack gypsum and are limited by the sodium content of subsurface waters. Therefore, the cement mineralogy reflects the progressive evaporation and contraction of subsurface brines from the edge of the pan where carbonate and gypsum cements are common to the centre of the pan where halite is the predominate cement.

Dolomitic nodules recovered from 3·45 m below the surface in Core 8 (Fig. 4) are laminated and contain diatom frustules and CFA as well as dolomite cement (Fig. 6A). The CFA occurs as elongate pods up to 1 μm in length similar in texture to Holocene CFA observed off Walvis Bay (Baturin, 2000). The dolomite occurs as submicrometer-sized crystals that together form 10 μm spherical clusters or pods (Fig. 6B); a texture observed for disseminated dolomite in offshore diatomaceous muds (Compton *et al.*, 2001). Many of the dolomite pods are associated with microbial sack-like structures with sheaths that extend outward and bifurcate (Fig. 6B). The microorganism represented by these structures may have played a role in the precipitation of the dolomite (Vasconcelos *et al.*, 1995; Vasconcelos & McKenzie, 1997; Wright, 1999; Wright & Wacey, 2005), although the structures are different from those described for bacteria associated with dolomitization in the seasonally evaporative Brazilian coastal lagoon Lagoa Vermelha (Vasconcelos & McKenzie, 1997).

The dolomitic nodules recovered in Core 8 occur in medium quartzose sand lacking organic matter and diatoms and were, therefore, probably reworked after their formation. Drilling of the pan, to depths of up to 65 m by Namdeb at the southern end of the pan, intercepted organic-rich muddy sand layers up to several metres thick that indicate earlier periods of high productivity. The age of the dolomitic nodules from Core 8 is probably older than the 6·3 ka dated shell fragments located 0·8 m upcore (Fig. 4). The presence of diatoms and barite crystals in the dolomite–CFA nodules suggests that the nodules formed during early diagenesis of sediment deposited when the area had a high biological productivity. Before deposition of the overlying aeolian sand, the Anichab depression would have been repeatedly submerged between 125 and 80 ka (Oxygen Isotope Stage 5) when sea level ranged from *ca* 50 m below to 5 m above present day (Cutler *et al.*, 2003). Anichab may have then been a highly productive lagoon or estuary whose organic-rich sediments were buried and preserved by the deposition of aeolian sands when the area became emergent during the lowered sea level of the glacial period from 80 to 7 ka. Therefore, a Late Pleistocene age is tentatively proposed for the dolomite recovered in Core 8.

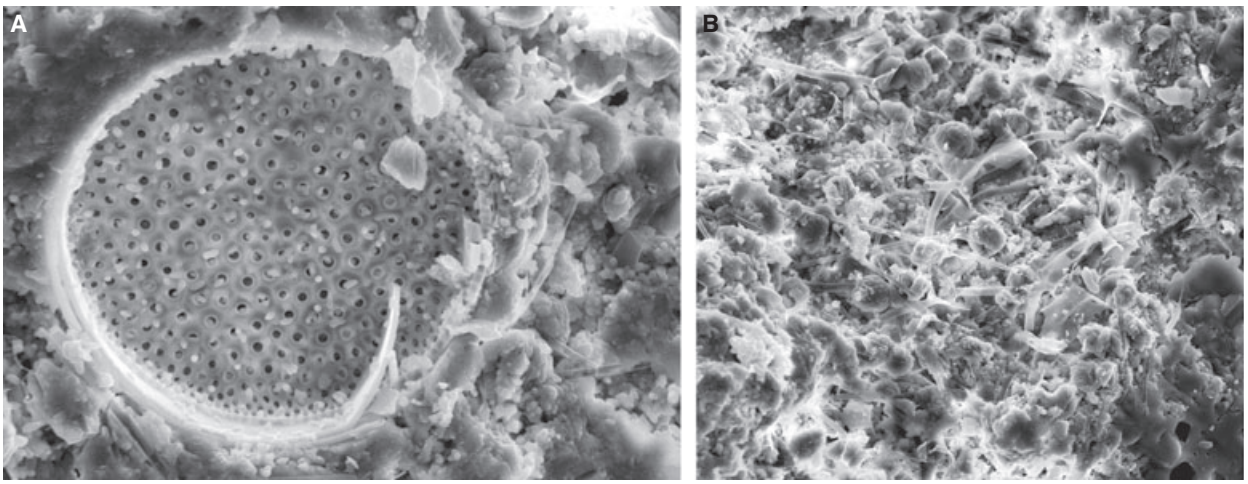

Fig. 6. SEM photomicrographs showing (A) carbonate fluorapatite crystals associated with a diatom frustule (40 μm in diameter) and (B) pod-shaped dolomite crystal clusters associated with microbial sheaths from a cemented nodule recovered from Core 8 at 3·45 m (field of view 100 μm).

The calcite cement from nodules recovered from Core 4 has Sr isotope ratios similar to the subsurface pan waters and sea water (Table 4), suggesting that Sr from the dissolution of shell fragments in the sand dominates over any radiogenic Sr in the groundwater. The aragonite and dolomite cements from nodules recovered from Core 8 have Sr isotope ratios higher than seawater perhaps reflecting Sr derived from the local runoff from Precambrian bedrock. Dolomite recovered from the shelf depressions offshore of Anichab Pan has Sr ratios significantly greater than sea water (Compton *et al.*, 2001) and suggests that these shelf areas at the time of dolomitization were completely emergent during sea-level lowstands, unlike the near present-day sea-level elevation of Anichab Pan.

The apparent absence of Holocene dolomite from Anichab Pan therefore suggests that the pan is not an appropriate modern analogue to the formation of upper Pleistocene dolomite found offshore on the shelf. The results of this study, however, show the important role of groundwater in the precipitation of early carbonate cements in the south-eastern area of the pan (Core 4). Pleistocene dolomite on the shelf to the north and south of the Anichab headland occurs in sediment-filled depressions thought to represent erosional river channels (O'Shea, 1971) or yardang troughs eroded by wind during sea-level lowstands. As with the Coorong area of south-east Australia, carbonate precipitation is favoured by the evaporation of groundwaters relatively high in alkalinity and calcium (von der Borch, 1976) and, more importantly in the case of dolomite formation, microbial sulphate reduction (Wright, 1999; Wright & Wacey, 2005).

The source of the groundwater to the south-eastern pan area (Core 4) is uncertain, but may represent regional drainage from the inland escarpment that flows on bedrock below the sand dunes between Koichab Pan located 30 km inland and the coast (Fig. 1B). These groundwater seeps commonly follow bedrock river channels or are focused in bedbrock depressions such as yardang troughs to form carbonate-cemented conglomerate or sandstone (Compton *et al.*, 2001). As with evaporative terrestrial pans from the Darling Hills area 70 km north of Cape Town, carbonate precipitation is favoured by high alkalinity groundwaters, such as those recovered in Core 4 (sample 4; Table 1), but dolomite in the Darling Hills pans forms as a secondary recrystallization of calcite and aragonite only after the Mg/Ca ratio has increased (Smith & Compton, 2004). Subsurface water from the south-eastern area of the pan has a Mg/Ca ratio of only 1 (sample 4; Table 1) and may explain why carbonate cements in Core 4 are low-Mg calcite. Holocene environments of Anichab Pan appear to have been largely subtidal to coastal at elevations near sea level. Diagenetic carbonate precipitation was limited in these environments because of an insufficient flux of carbonate alkalinity from groundwater seepage into the pan and insufficient burial and microbial degradation of organic matter.

CONCLUSIONS

The sediments of Anichab Pan provide new insights into Holocene sea-level fluctuations, mollusc biogeography and the origin of carbonate cements for comparison to both regional and global records. Anichab Pan is a sediment-filled depression similar to other north–south-oriented yardang troughs located onshore and offshore on the southern Namibian margin. The pan was most recently inundated during the mid-Holocene sea-level highstand 7 ka when the seaward yardang ridge, composed of Precambrian basement rock, was an island that provided sheltered subtidal sandy environments along this high-energy coast. The mollusc assemblage that inhabited the inundated aeolian sandbanks from 6·3 to 4·9 ka is similar to that of present-day sands leeward of coastal islands but includes warm-water molluscs such as the oyster *Ostreola stentina* and the bivalves *Gastrana matadoa* and *Solen capensis* which no longer live along this coast. The pan has been emergent since 4·9 ka in response to margin uplift in response to glacio-hydro-isostatic adjustments and the build up of coastal beach and dune sand deposits. Since emergence, wind erosion has been limited by the evaporative salt crusts in low areas of the pan and by the armouring of the elevated sandbanks by abundant in place mollusc shell.

The chemistry of subsurface pan waters indicates a predominantly seawater source modified by evaporation and the precipitation of carbonate, gypsum and halite towards the centre of the pan. Precipitation of carbonate minerals is limited by alkalinity, gypsum precipitation is limited by calcium and halite precipitation is limited by sodium. The subsurface water from the south-east corner of the pan is brackish and its relatively high Ca and alkalinity promote the formation of calcite cement associated with soil

organic matter degradation. Aragonite-cemented nodules occur in brine waters associated with shelly sands from the centre of the pan. Recovery of a reworked dolomite–CFA-cemented diatomaceous mudstone from the pan indicates productive estuarine or lagoon environments possibly during the Late Pleistocene before the depression became emergent and filled with aeolian sand. Therefore, the pan does not represent a modern analogue to sediment-filled depressions on the Namibian continental shelf that commonly contain dolomite of mixed-water origin. The absence of modern dolomite from the pan appears to reflect its elevation near sea level, the low organic matter content of pan sediments, and the low influx of alkaline groundwater.

ACKNOWLEDGEMENTS

Research was funded by the National Research Foundation and the University Research Council. I thank R. Spaggiari and Namdeb for providing logistical support for fieldwork, the Strausses for their hospitality, and M. Smith and G. Grobbelaar for assistance in the field. J. Pether and I. McMillan assisted in the identification of the macro and microfossils and reviewers D. Wright and F. Eckardt provided useful comments and suggestions.

REFERENCES

Baturin, G.N. (2000) Formation and evolution of phosphorite grains and nodules on the Namibian shelf, from Recent to Pleistocene. In: *Marine Authigenesis: From Global to Microbial* (Eds C.R. Glenn, L. Prevot-Lucas and J. Lucas), *SEPM Spec. Publ.*, **66,** 185–199.

Baxter, A.J. and **Meadows, M.E.** (1999) Evidence for Holocene sea level change at Verlorenvlei, Western Cape, South Africa. *Quatern. Int.*, **56,** 65–79.

von der Borch, C.C. (1976) Stratigraphy and formation of Holocene dolomitic carbonate deposits of the Coorong area, South Australia. *J. Sed. Petrol.*, **46,** 952–966.

Branch, M.L. and **Branch, G.M.** (1981) *The Living Shores of Southern Africa*. C. Struik, CapeTown, 272 pp.

Branch, G.M., Griffiths, C.L., Branch, M.L. and **Beckley, L.E.** (1994) *Two Oceans, a Guide to the Marine Life of Southern Africa*. David Philip, Cape Town, 360 pp.

Clark, J.A. and **Lingle, C.S.** (1979) Predicted relative sea-level changes (18,000 years B.P. to Present) caused by late-glacial retreat of the Antarctic ice sheet. *Quatern. Res.*, **11,** 279–298.

Compton, J.S. (2001) Holocene sea-level fluctuations inferred from the evolution of depositional environments of the southern Langebaan Lagoon salt marsh, South Africa. *Holocene*, **11,** 395–405.

Compton, J.S. (2006) The mid-Holocene sea-level highstand at Bogenfels Pan on the southwest coast of Namibia. *Quatern. Res.*, doi: 10.1016/j.yqres.2006.05.002.

Compton, J.S., Harris, C. and **Thompson, S.** (2001) Pleistocene dolomite from the Namibian shelf: high $^{87}Sr/^{86}Sr$ and $\delta^{18}O$ values indicate an evaporative, mixed-water origin. *J. Sed. Res.*, **71,** 800–808.

Cutler, K.B., Edwards, R.L., Taylor, F.W., Cheng, H., Adkins, J., Gallup, C.D., Cutler, P.M., Burr, G.S. and **Bloom, A.L.** (2003) Rapid sea-level fall and deep-ocean temperature change since the last interglacial period. *Earth Planet. Sci. Lett.*, **206,** 253–271.

Ehleringer, J.R. (1989) Carbon isotope ratios and physiological processes in arid land plants. In: *Stable Isotopes in Ecological Research* (Eds. P.W. Rundel, J.R. Ehleringer and K.A. Nagy). Ecological Studies, **68,** 41–54. Springer, New York.

Fleming, K., Johnston, P., Zwartz, D., Yokoyama, Y., Lambeck, K. and **Chappell, J.** (1998) Refining the eustatic sea-level curve since the Last Glacial Maximum using far- and intermediate-field sites. *Earth Planet. Sci. Lett.*, **163,** 327–342.

Hughen, K., Lehman, S., Southon, J., Overpeck, J., Marchal, O., Herring, C. and **Turnbull, J.** (2004) ^{14}C activity and global carbon cycle changes over the past 50,000 years. *Science*, **303,** 202–207.

Kaiser, E. (1926) *Die Diamantenwüste Südwestafrikas*. Dietrich Reimer, Berlin.

Kilburn, R. and **Rippey, E.** (1982) *Sea Shells of Southern Africa*. Macmillan South Africa, Johannesburg, 249 pp.

Kröner, A. and **Jackson, M.P.A.** (1974) Geological reconnaissance of the coast between Lüderitz and Marble Point, South West Africa. In: *Contributions to the Precambrian Geology of Southern Africa: A Volume in Honour of John de Villiers* (Ed. A. Kröner), Chamber of Mines, Precambrian Research Unit, South Africa, Bulletin 15, pp. 79–103.

Miller, D.E., Yates, R.J., Parkington, J.E. and **Vogel, J.C.** (1993) Radiocarbon-dated evidence relating to a mid-Holocene relative high sea-level on the south-western Cape coast, South Africa. *S. Afr. J. Sci.*, **89,** 35–44.

O'Shea, D.O'C. (1971) *An outline of the inshore submarine geology of southern South West Africa and Namaqualand*. Unpubl. M.Sc. Thesis, University of Cape Town, Rondebosch, South Africa, 101 pp.

Pierre, C., Ortlieb, L. and **Person, A.** (1984) Supratidal evaporitic dolomite at Ojo de Liebre Lagoon: mineralogical and isotopic arguments for primary crystallization. *J. Sed. Petrol.*, **54,** 1049–1061.

Ramsay, P.J. and **Cooper, J.A.G.** (2002) Late Quaternary sea-level change in South Africa. *Quatern. Res.*, **57,** 82–90.

Rogers, J. (1977) *Sedimentation on the Continental Margin off the Orange River and the Namib Desert*. Marine Geoscience Group, University of Cape Town, Rondebosch, South Africa, Bulletin No. 7, 162 pp.

Smith, M. and **Compton, J.S.** (2004) Origin and evolution of major salts in the Darling Pans, Western Cape, South Africa. *Appl. Geochem.*, **19,** 645–664.

Stuiver, M. and **Braziunas, T.F.** (1993) Modeling atmospheric ^{14}C influences and ^{14}C ages of marine samples to 10,000 BC. *Radiocarbon*, **35,** 137–189.

Talma, S. and **Vogel, J.C.** (1993) A simplified approach to calibrating ^{14}C dates. *Radiocarbon*, **35,** 317–322.

Tonner, T.W.W. (2003) A spatial database for the Later Stone Age site 'Dunefield Midden,' (Western Cape, South Africa).

Unpubl. M.Sc. Thesis, University of Cape Town, Rondebosch, South Africa, 290 pp.

Vasconcelos, C. and **McKenzie, J.A.** (1997) Microbial mediation of modern dolomite precipitation and diagenesis under anoxic conditions (Lagoa Vermelha, Rio de Janeiro, Brazil). *J. Sed. Res.*, **67,** 378–390.

Vasconcelos, C., McKenzie, J.A., Bernasconi, S., Grujic, D. and **Tien, A.J.** (1995) Microbial mediation as a possible mechanism for natural dolomite formation at low temperatures. *Nature*, **377,** 220–222.

Wright, D.T. (1999) The role of sulphate-reducing bacteria and cyanobacteria in dolomite formation in distal ephemeral lakes of the Coorong region, South Australia. *Sed. Geol.*, **126,** 147–157.

Wright, D.T. and **Wacey, D.** (2005) Dolomite precipitation in experiments using sulphate reducing bacterial populations in simulated lake and pore waters from distal ephemeral lakes, Coorong region, South Australia. *Sedimentology*, **52,** 987–1008.

Manuscript received 2 November 2005; revision accepted 11 July 2006

